

IMPROVED TURBULENCE AND TRANSITION CLOSURES FOR SEPARATED FLOWS

Joachim Hodara
Ph.D. Candidate

Marilyn J. Smith
Professor

School of Aerospace Engineering
Georgia Institute of Technology
Atlanta, Georgia, 30332-0150, USA

ABSTRACT

A new turbulence approach is proposed that combines the strengths of Unsteady Reynolds-Averaged Navier-Stokes (URANS) and Large Eddy Simulation (LES) turbulence closure with local dynamic kinetic model (LDKM) and the widely adopted $\gamma - \overline{Re_{\theta_t}}$ transition model. This method has the potential for accurately capturing massively separated boundary layers in the transitional Reynolds number range at a reasonable computational cost, and therefore holds great promise for the rotorcraft industry. Comparisons are evaluated on several cases, including a transitional flat plate, circular cylinder in crossflow and NACA 63-415 wing. Cost and accuracy correlations with URANS and prior hybrid URANS-LES approaches with and without transition modeling indicate that this new method can capture both separation and transition more accurately and cost effectively.

NOTATION

c	Airfoil chord length (m)
\mathbf{D}	Differential operator
\mathbf{E}	Statistical operator
\mathbf{F}	Filtering operator
\mathcal{F}	Blending factor, $0 \leq \mathcal{F} \leq 1$
\mathbf{H}	Additive hybrid operator
\mathcal{K}	Hybrid kinetic energy
M	Mach number, $M = V/a$
Pr	Prandtl number, $Pr = C_p \mu / k$
Re	Reynolds number, $Re = \rho V c / \mu$
$\overline{Re_{\theta_t}}$	Transition onset Reynolds number
S	Mean strain rate, $S = (2S_{ij}S_{ij})^{1/2}$
Tu	Turbulence intensity (%)
u	Velocity (m/s)
y	Distance to the nearest wall (m)
α	Angle of attack (rad)
Δ	Local grid spacing (m)
γ	Intermittency
μ	Molecular viscosity (Pa.s)
ρ	Density (kg/m^3)
ω	Specific dissipation rate (1/s)
Ω	Vorticity magnitude, $\Omega = (2\Omega_{ij}\Omega_{ij})^{1/2}$
$\langle . \rangle$	Filtered quantity
$\{.\}$	Favre-filtered quantity

SUPER/SUBSCRIPTS

E	RANS filtered
F	LES filtered
H	Hybrid filtered
∞	Freestream condition

1 INTRODUCTION

The aerodynamic behavior of modern rotorcraft is highly complex and has proven to be an arduous challenge for Computational Fluid Dynamics (CFD). Flow features such as massively separated boundary layers or transition to turbulence are common in industrial applications and need to be accurately captured in order to predict the rotor performance. Recent advances in numerical methods and turbulence modeling have made progress in resolving each of these issues independent of the other, but the flow physics of many configurations requires that combined approaches be applied. State-of-the-art hybrid RANS-LES (HRLES) turbulence closures have shown great promise in capturing the unsteady flow details and integrated performance quantities for complex stalled flows^[1-3]. Similarly, the correlation-based transition model of Langtry and Menter has been successfully applied to a wide range of applications involving attached or mildly separated flows, including turbine blades and finite wings^[4-6]. However, there still lacks an unified approach that could

tackle massively separated flows in the transitional flow region. In this effort, the two approaches have been combined to yield a methodology capable of accurately predicting the features in these highly complex unsteady turbulent flows at a reasonable computational cost.

2 TRANSITIONAL HRLES MODEL

2.1 Hybrid RANS-LES Modeling

Despite the recent progress in numerical algorithms and hardware, Large-Eddy Simulation (LES) remains too costly for most industrial applications^[7]. Hybrid RANS-LES closures have recently emerged as a promising alternative for capturing complex turbulent flows at a moderate cost. The separated flows and wakes are captured using LES while attached boundary layers near the walls are resolved by exploiting the best of RANS modeling. Many approaches to couple these two representations of the turbulent field have already been proposed in the literature, a review of which can be found in Fröhlich^[8]. The most widely used hybrid RANS-LES closure is the Detached-Eddy Simulation (DES)^[3], for which a single turbulence model is applied to both the RANS and LES regions. The model switches between RANS and LES by controlling the turbulent length scale for the destruction term in the eddy viscosity equation. In the original DES, the RANS to LES transition (RTLTL) zone is purely determined by the local grid resolution, which may result in severe constraints on the grid quality as well as non-convergence of the results upon progressive refinement of the mesh. More importantly, this grid dependency is responsible for Modeled-Stress Depletion (MSD) when the mesh is small enough to trigger the DES limiter, but not small enough to support the LES content. This premature transition to LES is often characterized by a grid-induced separation of the boundary layer. Modified versions of DES have been proposed to tackle these issues, such as Delayed DES (DDES)^[9] and Improved DDES (IDDES)^[10]. These modifications are primarily empirical, and the model still lacks a proper mechanism to transport the momentum in the RTLTL zone. As a consequence, Piomelli et al.^[11] identified long streaks near the walls that were unable to transfer their wall-normal momentum to the outer-boundary layer due to the absence of fluctuations in the RANS region. Piomelli et al. introduced a stochastic forcing term in the RTLTL zone to mimic the turbulent transfer of momentum, resulting in dramatically improved correlations throughout the boundary layer. Other authors such as Deck^[12] have been developing a zonal formulation of DES (ZDES) that avoids MSD by explicitly marking the RANS and LES regions. Although this approach

performed well for relatively simple geometries^[2,12], some questions remain unanswered regarding the extension of the method to complex three-dimensional problems.

In order to remove the need to introduce artificial turbulent fluctuations in the RTLTL zone, Germano^[13,14] proposed a hybrid RANS-LES framework based on an additive hybrid filter:

$$(1) \quad \mathbf{H} = \mathcal{F}\mathbf{E} + (1 - \mathcal{F})\mathbf{F}$$

where \mathbf{E} and \mathbf{F} represent the statistical and filtering operators, respectively. \mathcal{F} is a blending factor that can be a function of both space and time. Germano demonstrated that applying the hybrid operator to the Navier-Stokes equations resulted in hybrid terms that were function of the RANS and LES fields only (as opposed to the hybrid field). His approach was extended to compressible flows by Sánchez-Rocha^[15], who also conducted an in-depth analysis of these new hybrid terms. Sánchez-Rocha concluded that these terms played an important role in the simulation by ensuring a proper transfer of momentum in the RTLTL zone, hence removing the need for any stochastic forcing. Nevertheless, these hybrid terms have primarily been neglected in the literature to date due to their relatively complex formulation. This simplified hybrid RANS-LES closure (neglecting these hybrid terms) has performed very well over a wide range of turbulent configurations, including complex rotating hubs^[1] and wings in the post-stall regime^[16].

In the present work, a new approach for capturing transitional separated flows is proposed based on the hybrid operator. While the final model will remove the homogeneous assumption for the blending factor \mathcal{F} , it was decided for the present analysis to investigate the simplified version only. Once the viability and robustness of the new method have been confirmed, the hybrid terms will be fully incorporated to yield a rigorous mathematical representation of the turbulent flow field.

2.2 Transition Modeling

There are few methods currently capable of accurately predicting transitional boundary layers over complex geometries at a reasonable computational cost. LES has been successfully employed to capture transitional flows^[17,18], but the transition location was found to be very sensitive to the choice of the Smagorinsky constant. This issue has been mitigated by the introduction of dynamic models^[19], as the eddy viscosity naturally reduces to zero in laminar regions^[20]. Nevertheless, while LES predicts the correct qualitative flow field, quantitative comparisons have highlighted some discrepancies with experimental and DNS data^[21]. Furthermore,

the computational cost of LES remains too intensive for most engineering applications. Linear methods such as the e^N [22, 23] approach provide accurate transitional predictions, but their applications are limited to natural transition cases without reattachment bubbles and their implementation poses several challenges for complex three-dimensional configurations. The same conclusion applies to methods based on empirical correlations for transition onset [24, 25]. Although these approaches are very attractive due to their accurate transition predictions, their dependency on momentum-thickness Reynolds number makes them unsuitable for complex three-dimensional configurations. Also present in the literature, Low-Reynolds-Number turbulence models [26, 27] and models based on a transport equation for the laminar kinetic energy [28] typically suffer from unreliable predictions and do not have the correct sensitivity to pressure gradients.

Langtry and Menter [29] in 2006 proposed a correlation-based model which captures the correct transitional behavior while remaining fully local. The vorticity Reynolds number, a local parameter readily available in most solvers, is used to trigger the transition process. Originally based on the Menter $k - \omega$ Shear Stress Transport (SST) model [30], this method includes two additional partial differential equations for the transport of intermittency γ and transition Reynolds number based on the momentum thickness, \bar{Re}_{θ} . The $\gamma - \bar{Re}_{\theta}$ correlation-based model has been widely applied over the last decade, primarily due to its local nature and accurate predictions of transitional flows [4, 5, 31–33].

2.3 Proposed Transitional HRLES Model

Sánchez-Rocha [15] developed a hybrid RANS-LES model based on the additive filter concept introduced by Germano [14]. The original approach relies on the $k - \omega$ SST model [30] for the URANS region and the one-equation localized dynamic model (LDKM) [34] for the LES region. Both these models include an additional transport equation for the turbulent kinetic energy (k for URANS and k^{sgs} for LES) so that a new equation for the hybrid turbulent kinetic energy $\mathcal{K} = \mathcal{F}k + (1 - \mathcal{F})k^{sgs}$ can also be derived. This model has been successfully extended to legacy URANS solvers and shown to provide improved separation and performance for canonical and rotorcraft configurations, for example cylinders [16], rotor blades [16] and rotor hubs [1]. In the present work, the approach of Sánchez-Rocha is extended to transitional flows by applying the $\gamma - \bar{Re}_{\theta}$ correlation-based model of Langtry and Menter [4] in the URANS region and combining it with the LDKM in the LES region. Such method should therefore be capable to provide accurate predictions for massively separated

flows, as well as boundary layers in the transitional regime. A similar approach was recently suggested by Sorensen [33], who combined the URANS transition model with a DDES model and obtained improved correlations on circular cylinders in the transitional regime. Sorensen also tested his model on a semi-infinite S809 wing at the onset of stall, but the results proved inconclusive as the configuration was more sensitive to the turbulence production mechanisms at the wall. In this configuration an inaccurate transfer of momentum and energy has a more pronounced impact on the solution, as compared to a blunt body where the separation point is fixed by a geometric discontinuity. It is therefore proposed that a model based on the additive filter concept of Germano [14] will provide more consistent results without requiring additional stochastic turbulent forcing near the surface.

In order to derive the hybrid Navier-Stokes equations, a number of key assumptions are typically made regarding the behavior of the statistical and filtering operators:

- The statistical and filtering operators \mathbf{E} and \mathbf{F} commute with the differentiation operator \mathbf{D} (which can be spatial or temporal): $\mathbf{D}\mathbf{F} = \mathbf{F}\mathbf{D}$ and $\mathbf{D}\mathbf{E} = \mathbf{E}\mathbf{D}$.
- The filtering operator applied to a filtered variable does not recover the same filtered variable ($\mathbf{F}\mathbf{F} \neq \mathbf{F}$), but the statistical operator does ($\mathbf{E}\mathbf{E} = \mathbf{E}$). Also, applying the statistical operator to the filtered variable recovers the statistical variable ($\mathbf{E}\mathbf{F} = \mathbf{E}$).
- The blending factor \mathcal{F} commutes with the statistical operator \mathbf{E} ($\mathcal{F}\mathbf{E} = \mathbf{E}\mathcal{F}$). This last assumption is more demanding than the rest, but can be justified by considering the flexible definition of the statistical operator as applied to turbulent flows [35].

These assumptions allow for the statistical variables to be recovered from the hybrid field, as shown in the following equation:

$$(2) \quad \mathbf{E}\mathbf{H} = \mathbf{E}[\mathcal{F}\mathbf{E}] + \mathbf{E}[(1 - \mathcal{F})\mathbf{F}] = \mathbf{E}.$$

Another important consideration to keep in mind is that the hybrid operator does not commute with the differentiation operator if the blending factor \mathcal{F} is space or time dependent.

$$(3) \quad \mathbf{H}\mathbf{D} = \mathbf{D}\mathbf{H} + \mathbf{D}[\mathcal{F}](\mathbf{F} - \mathbf{E}).$$

The fact that these two operators do not commute introduces a large number of additional terms in the hybrid Navier-Stokes equations. In order to illustrate the

concept of hybrid RANS-LES filtering, the additive operator is applied to the continuity equation

$$(4) \quad \partial_t \rho + \partial_j (\rho u_j) = 0,$$

which becomes

$$(5) \quad \partial_t \langle \rho \rangle_H + \partial_j \langle \rho u_j \rangle_H = \sigma_\rho$$

with

$$(6) \quad \sigma_\rho = \frac{\partial \mathcal{F}}{\partial t} (\langle \rho \rangle_E - \langle \rho \rangle_F) + \frac{\partial \mathcal{F}}{\partial x_j} (\langle \rho u_j \rangle_E - \langle \rho u_j \rangle_F).$$

Similar terms arise in the other conservation equations after application of the hybrid operator. The numerical code solves the hybrid variables, so that the statistical and filtered quantities must be reconstructed to compute the hybrid terms such as σ_ρ in Eq. (6). It has already been illustrated in Eq. (2) that the statistical field can be recovered by applying the statistical operator to the hybrid variables. In theory, the LES content can be obtained by slightly rearranging Eq. (2) to yield

$$(7) \quad \mathbf{F} = \frac{\mathbf{H} - \mathcal{F}\mathbf{E}}{1 - \mathcal{F}}.$$

Unfortunately, this type of inverse filtering operation is generally ill-conditioned, as the filtered variables diverge in RANS region when $\mathcal{F} \rightarrow 1$. Rajamani^[36] was able to avoid the issue by selecting a blending function with a lower limit of 0.15, and obtained good agreement with experimental and DNS data for a turbulent channel flow. Instead of reconstructing the LES content using Eq. (7), Sánchez-Rocha^[37] proposed to close the hybrid equations by modeling the filtered variables using order-of-magnitude estimations. Sánchez-Rocha tested his approach on a turbulent flat plate case and obtained favorable comparison with published data while improving the robustness of the original method. To date, the reconstruction of the LES field from the hybrid variables is still an active field of research, which has been investigated almost exclusively on simple canonical cases. In the present study, it has therefore been decided to neglect these terms in the hybrid equations, a successful practice demonstrated for complex turbulent simulations^[1, 16]. Once the baseline concept has been validated, it will become possible to implement these terms with relative ease to improve the transfer of momentum in the RTLT zone.

Applying the additive filter \mathbf{H} to the original set of Navier-Stokes equations while assuming the blending factor \mathcal{F} to be homogeneous, the new hybrid conservation equations are obtained:

$$(8) \quad \partial_t \langle \rho \rangle_H + \partial_j (\langle \rho \rangle_H \{u_j\}_H) = 0$$

$$(9) \quad \begin{aligned} & \partial_t (\langle \rho \rangle_H \{u_i\}_H) + \partial_j (\langle \rho \rangle_H \{u_j\}_H \{u_i\}_H) = \\ & \partial_j \left(-\langle p \rangle_H \delta_{ij} + \{\sigma_{ij}\}_H + \tau_{ij}^H \right) \end{aligned}$$

$$(10) \quad \begin{aligned} & \partial_t (\langle \rho \rangle_H \{E\}_H) + \partial_j (\langle \rho \rangle_H \{u_j\}_H \{H\}_H) = \\ & \partial_j \left(-\{q_j\}_H + \{u_i\}_H \{\sigma_{ij}\}_H + \{u_i\}_H \tau_{ij}^H \right), \end{aligned}$$

where the hybrid Favre-filtered variables $\{\cdot\}_H$ have been introduced. The thermodynamic variables are related through the perfect gas law ($\langle p \rangle_H = \langle \rho \rangle_H R \{T\}_H$) and the molecular viscosity is obtained using Sutherland's law. The fluid is assumed to be Newtonian, so that the viscous stresses $\{\sigma_{ij}\}_H$ are proportional to the strain-rates $\{s_{ij}\}_H = \frac{1}{2} (\partial_j \{u_i\}_H + \partial_i \{u_j\}_H)$. Similarly, the hybrid turbulent stresses τ_{ij}^H are obtained using an eddy viscosity and a gradient diffusion assumption, such that

$$(11) \quad \{\sigma_{ij}\}_H = 2\mu \{s_{ij}\}_H$$

$$(12) \quad \tau_{ij}^H = 2\mu_T \left(\{s_{ij}\}_H - \frac{1}{3} \partial_k \{u_k\}_H \delta_{ij} \right) - \frac{2}{3} \langle \rho \rangle_H \mathcal{K} \delta_{ij}.$$

The total energy in Eq. (10) is given by

$$(13) \quad \{E\}_H = \frac{\langle p \rangle_H}{\gamma - 1} + \frac{1}{2} \langle \rho \rangle_H \{u_i\}_H \{u_i\}_H + \langle \rho \rangle_H \mathcal{K},$$

and is related to the total enthalpy via the relation $\{H\}_H = \{E\}_H + \langle p \rangle_H / \langle \rho \rangle_H$. Finally, a Reynolds analogy is used to model the heat flux vector in Eq. (10):

$$(14) \quad \begin{aligned} \{q_j\}_H = & -(\kappa + \mu_T C_p / Pr_T) \partial_j \{T\}_H \\ & - (\mu + \sigma^* \mu_T) \partial_j \mathcal{K}. \end{aligned}$$

Equation (14) also includes the terms associated with the molecular diffusion and turbulent transport. The turbulent Prandtl number Pr_T and turbulent transport coefficient σ^* are given the values 0.9 and 0.5, respectively. Providing the blending function \mathcal{F} is assumed to be homogeneous in space and time, the hybrid equations Eq. (8) to (10) have a form similar to the RANS or filtered equations, but the meaning of the various terms is now different. As expected, the closure problem arises and a model must be devised to approximate the eddy viscosity μ_T .

As discussed in the previous sections, the $\gamma - \overline{Re_\theta}$ correlation-based transition model^[4] is coupled to the one-equation localized dynamic model (LDKM)^[34]. Both these models include an additional transport equation for the turbulent kinetic energy so that a new equation for the hybrid turbulent kinetic energy \mathcal{K} can be derived. As the rigorous combination of two models does not guarantee an improved formulation, the transport equation for the hybrid turbulent kinetic energy is simply devised to recover the RANS and LES equations as the blending factor \mathcal{F} goes to one or zero, respectively. It follows that:

$$(15) \quad \partial_t (\langle \rho \rangle_H \mathcal{K}) + \partial_j (\langle \rho \rangle_H \{u_j\}_H \mathcal{K} - K_j^T) = K^S,$$

where

$$(16) \quad K_j^T = [\mu + \mathcal{F} \sigma_k \mu^E + (1 - \mathcal{F}) \mu^F / C_1] \partial_j \mathcal{K}$$

$$(17) \quad K^S = \mathcal{F} \left(\gamma_{\text{eff}} \bar{P}_k^E - \bar{\gamma}_{\text{eff}} \beta^* \langle \rho \rangle_H \omega \mathcal{K} \right) + (1 - \mathcal{F}) \left(\tau_{ij}^F \partial_j \{u_i\}_H - C_\varepsilon \langle \rho \rangle_H \mathcal{K}^{3/2} / \Delta \right),$$

where the RANS production term is limited to ten times the values of the local RANS dissipation to prevent the build-up of turbulent kinetic energy in stagnation regions^[30], so that

$$(18) \quad \bar{P}_k^E = \min(\tau_{ij}^E \partial_j \{u_i\}_H, 10 \beta^* \langle \rho \rangle_H \omega \mathcal{K}).$$

The two models have been linearly blended and all occurrences of k and k^{sgs} have been substituted by the hybrid turbulence kinetic energy \mathcal{K} . The RANS production and destruction terms have also been modified to include the intermittency γ_{eff} as defined in the correlation-based model^[4]. In some cases, the intermittency is permitted to increase beyond a value of one to improve reattachment predictions. However, its value is limited in the destruction term of Eq. (17) so that $\bar{\gamma}_{\text{eff}} = \min[\max(\gamma_{\text{eff}}, 0.1), 1.0]$. The Reynolds and subgrid-scale (SGS) stresses are both assumed to follow the gradient diffusion assumption, which yields

$$(19) \quad \tau_{ij}^E = 2\mu^E \left(\{s_{ij}\}_H - \frac{1}{3} \partial_k \{u_k\}_H \delta_{ij} \right) - \frac{2}{3} \langle \rho \rangle_H \mathcal{K} \delta_{ij}$$

$$(20) \quad \tau_{ij}^F = 2\mu^F \left(\{s_{ij}\}_H - \frac{1}{3} \partial_k \{u_k\}_H \delta_{ij} \right) - \frac{2}{3} \langle \rho \rangle_H \mathcal{K} \delta_{ij}$$

All the coefficients in Eq. (15) have been kept identical to their original values^[4], and the $k - \omega$ SST coefficients, ϕ , are still obtained by blending the $k - \varepsilon$ (1) and $k - \omega$ (2) constants as follows:

$$(21) \quad \phi = F_1 \phi_1 + (1 - F_1) \phi_2 \quad ; \quad F_1 = \max(F_1^{SST}, F_3)$$

$$(22) \quad F_1^{SST} = \tanh(\arg_1^4) \quad ; \quad F_3 = e^{-\left(\frac{R_y}{120}\right)^8} \quad ; \quad R_y = \frac{\langle \rho \rangle_H \sqrt{\mathcal{K}} y}{\mu}$$

$$\arg_1 = \min \left[\max \left(\frac{\sqrt{\mathcal{K}}}{\beta^* \omega y}, \frac{500\nu}{y^2 \omega} \right), \frac{4 \langle \rho \rangle_H \sigma_{\omega 2} \mathcal{K}}{CD_{k\omega} y^2} \right]$$

$$CD_{k\omega} = \max(2 \langle \rho \rangle_H \sigma_{\omega 2} / \omega \partial_j \omega \partial_j \mathcal{K}, 10^{-10})$$

The function F_3 was introduced in the transition model of Langtry-Menter to prevent F_1 from reducing to zero in laminar regions^[4]. The distance to the nearest wall is denoted y and the local grid spacing Δ is approximated by the cubic root of the cell volume. The model coefficients are as follows:

$$(23) \quad \sigma_{k1} = 0.85 \quad ; \quad \sigma_{k2} = 1.0 \quad ; \quad \beta^* = 0.09$$

$$\sigma_{\omega 1} = 0.5 \quad ; \quad \sigma_{\omega 2} = 0.856 \quad ; \quad C_\varepsilon = 0.916$$

The LES coefficients can either be given constant values or be obtained dynamically as part of the solution, following the approach of Kim & Menon^[34]. In the present work, the first option (constant coefficients) was selected. The correlation-based model includes three additional transport equations for the specific dissipation rate ω , intermittency γ and transition onset Reynolds number \overline{Re}_{θ_t} , which are not present in the LES model. These equations are computed based on the hybrid variables so that the initial model is recovered when $\mathcal{F} \rightarrow 1$. The transport equation for the specific energy dissipation rate ω is defined as

$$(24) \quad \partial_t (\langle \rho \rangle_H \omega) + \partial_j (\langle \rho \rangle_H \{u_j\}_H \omega) = \langle \rho \rangle_H \alpha / \mu^E \bar{P}_k^E - \beta \langle \rho \rangle_H \omega^2 + \partial_j [(\mu + \sigma_\omega \mu^E) \partial_j \omega] + 2(1 - F_1) \langle \rho \rangle_H \sigma_{\omega 2} / \omega \partial_j \mathcal{K} \partial_j \omega$$

where the coefficients (blended using Eq.(21)) are given by

$$(25) \quad \alpha_1 = 5/9; \alpha_2 = 0.44; \beta_1 = 0.075; \beta_2 = 0.0828$$

The transport equation for the intermittency γ was proposed as follows by Langtry and Menter^[4]:

$$(26) \quad \partial_t (\langle \rho \rangle_H \gamma) + \partial_j (\langle \rho \rangle_H \{u_j\}_H \gamma) = P_\gamma - E_\gamma + \partial_j [(\mu + \mu^E / \sigma_f) \partial_j \gamma]$$

The production term is defined as

$$(27) \quad P_\gamma = F_{\text{length}} c_{a1} \langle \rho \rangle_H \langle S \rangle_H \sqrt{\gamma F_{\text{onset}}} (1 - c_{e1} \gamma)$$

where $\langle S \rangle_H = (2 \{s_{ij}\}_H \{s_{ij}\}_H)^{1/2}$ is the mean strain-rate invariant. The coefficients have been calibrated such that $c_{a1} = 2.0$, $c_{e1} = 1.0$ and $\sigma_f = 1.0$. The function F_{onset} is used to trigger the production of intermittency in the boundary layer, while the function F_{length} determines the length of the transitional region.

$$(28) \quad F_{\text{onset}1} = R_v / (2.193 R_{\theta_c})$$

$$F_{\text{onset}2} = \min[\max(F_{\text{onset}1}, F_{\text{onset}1}^4), 2.0]$$

$$F_{\text{onset}3} = \max[1 - (R_T / 2.5)^3, 0]$$

$$F_{\text{onset}} = \max(F_{\text{onset}2} - F_{\text{onset}3}, 0)$$

with

$$(29) \quad R_v = \frac{\langle \rho \rangle_H y^2 \langle S \rangle_H}{\mu} \quad ; \quad R_T = \frac{\langle \rho \rangle_H \mathcal{K}}{\mu \omega}$$

More details regarding the precise purpose of each term can be found in the 2009 publication of Langtry and Menter^[4]. The critical Reynolds number R_{θ_c} and transition length are obtained from empirical correlations, a review of which can be found in

$$(30) \quad R_{\theta_c} = \begin{cases} \overline{R_{\theta}} - \left(396.035 \times 10^{-2} - 120.656 \times 10^{-4} \overline{R_{\theta}} + 868.230 \times 10^{-6} \overline{R_{\theta}}^2 \right. \\ \quad \left. - 696.506 \times 10^{-9} \overline{R_{\theta}}^3 + 174.105 \times 10^{-12} \overline{R_{\theta}}^4 \right) & \text{if } \overline{R_{\theta}} \leq 1870 \\ \overline{R_{\theta}} - [593.11 + 0.482 (\overline{R_{\theta}} - 1870.0)] & \text{if } \overline{R_{\theta}} > 1870 \end{cases}$$

$$(31) \quad F_{length} = \begin{cases} 398.189 \times 10^{-1} - 119.270 \times 10^{-4} \overline{R_{\theta}} - 132.567 \times 10^{-6} \overline{R_{\theta}}^2 & \text{if } \overline{R_{\theta}} < 400 \\ 263.404 - 123.939 \times 10^{-2} \overline{R_{\theta}} + 194.548 \times 10^{-5} \overline{R_{\theta}}^2 - 101.695 \times 10^{-8} \overline{R_{\theta}}^3 & \text{if } 400 \leq \overline{R_{\theta}} < 596 \\ 0.5 - 3.0 \times 10^{-4} (\overline{R_{\theta}} - 596.0) & \text{if } 596 \leq \overline{R_{\theta}} < 1200 \\ 0.3188 & \text{if } \overline{R_{\theta}} \geq 1200 \end{cases}$$

Benyahia^[31]. In the present work, the correlations proposed by Langtry and Menter in 2009 were implemented, as observed in Eqs. (30) and (31). The destruction/relaminarization source term is defined as follows:

$$(32) \quad E_{\gamma} = c_{a2} \langle \rho \rangle_H \langle \Omega \rangle_H \gamma F_{turb} (c_{e2} \gamma - 1)$$

where $c_{a2} = 0.06$ and $c_{e2} = 50.0$. The local vorticity magnitude is defined as $\langle \Omega \rangle_H = (2\{\Omega_{ij}\}_H \{\Omega_{ij}\}_H)^{1/2}$, where the vorticity tensor is given by $\{\Omega_{ij}\}_H = \frac{1}{2} (\partial_j \{u_i\}_H - \partial_i \{u_j\}_H)$. The function F_{turb} is used to disable the destruction term in laminar boundary layers and viscous sublayers, such that

$$(33) \quad F_{turb} = \exp \left[- (R_T/4)^4 \right]$$

where R_T is the viscosity ratio defined in Eq. (29). In order to improve the reattachment predictions of the model, the intermittency is locally allowed to exceed a value of one, resulting in larger production of turbulent kinetic energy.

$$(34) \quad \gamma_{eff} = \max(\gamma, \gamma_{sep})$$

$$(35) \quad \gamma_{sep} = \min \{ s_1 \max [0, R_v / (3.235 R_{\theta_c}) - 1] F_{re}, 2 \} F_{\theta}$$

$$(36) \quad F_{re} = \exp \left[- (R_T/20)^4 \right] \quad ; \quad s_1 = 2$$

In order to preserve the local nature of the model, Langtry and Menter treated the transition onset Reynolds number R_{θ} as a local variable called $\overline{R_{\theta}}$, which they assumed to be governed by a standard transport equation. At the edge of the boundary layer, the equation is defined such that $\overline{R_{\theta}}$ recovers the value R_{θ} .

$$(37) \quad \begin{aligned} \partial_t (\langle \rho \rangle_H \overline{R_{\theta}}) + \partial_j (\langle \rho \rangle_H \{u_j\}_H \overline{R_{\theta}}) &= P_{\theta} \\ + \partial_j [\sigma_{\theta} (\mu + \mu^E) \partial_j \overline{R_{\theta}}] & \end{aligned}$$

$$(38) \quad P_{\theta} = c_{\theta} \langle \rho \rangle_H / t (R_{\theta} - \overline{R_{\theta}}) (1.0 - F_{\theta})$$

with $\sigma_{\theta} = 2.0$ and $c_{\theta} = 0.03$. The transition Reynolds number R_{θ} is obtained from experimental correlations, as a function of the turbulent intensity Tu (in %) and stream-wise pressure gradient parameter λ_{θ} , both evaluated at the edge of the boundary layer:

$$(39) \quad Tu = 100 \frac{\sqrt{2\mathcal{K}/3}}{\langle U \rangle_H} \quad ; \quad \lambda_{\theta} = \frac{\langle \rho \rangle_H \theta^2}{\mu} \frac{d\langle U \rangle_H}{ds}$$

where $\langle U \rangle_H = (\langle u_i \rangle_H \langle u_i \rangle_H)^{1/2}$ is the velocity magnitude and $d\langle U \rangle_H/ds = \langle u_i \rangle_H \langle u_j \rangle_H / \langle U \rangle_H^2 \partial_i \langle u_j \rangle_H$ is the stream-wise acceleration. The correlations are given in Eq. (40) and (41), where the parameters are typically limited as follows: $-0.1 \leq \lambda_{\theta} < 0.1$, $Tu \geq 0.027\%$ and $R_{\theta} \geq 20$. A fixed point iteration method is used to converge to the correct momentum thickness since the pressure-gradient parameter λ_{θ} is not known a priori. The parameter t in Eq. (38) is a dimensional parameter with the unit of time which was introduced to ensure that the source term would scale with the convective and diffusive terms. It is defined as follows:

$$(42) \quad t = 500\mu / (\langle \rho \rangle_H \langle U \rangle_H^2)$$

The function F_{θ} vanishes inside of boundary layers, so that the transition Reynolds number $\overline{R_{\theta}}$ is only convected and diffused.

$$(43) \quad F_{\theta} = \min \left[\max \left\{ F_w e^{-\left(\frac{\gamma}{\delta}\right)^4}, 1.0 - \left(\frac{\gamma - 1/c_{e2}}{1 - 1/c_{e2}}\right)^2 \right\}, 1.0 \right]$$

$$(44) \quad \delta = \frac{50 \langle \Omega \rangle_H \gamma}{\langle U \rangle_H} \delta_{BL} \quad ; \quad \delta_{BL} = \frac{15}{2} \theta_{BL} \quad ; \quad \theta_{BL} = \frac{\overline{R_{\theta}} \mu}{\langle \rho \rangle_H \langle U \rangle_H}$$

$$(45) \quad F_w = \exp \left[- \left(R_{\omega} / 10^5 \right)^2 \right] \quad ; \quad R_{\omega} = \langle \rho \rangle_H \omega y^2 / \mu$$

The RANS and SGS eddy viscosities are formulated as:

$$(46) \quad \mu^E = \frac{\langle \rho \rangle_H a_1 \mathcal{K}}{\max [a_1 \omega, \langle S \rangle_H F_2 \min (\gamma_{eff}, 1.0)]}$$

$$(40) \quad R_{\theta} = \begin{cases} (1173.51 - 589.428Tu + 0.2196Tu^{-2}) F(\lambda_{\theta}) & \text{if } Tu \leq 1.3\% \\ 331.5(Tu - 0.5658)^{-0.671} F(\lambda_{\theta}) & \text{if } Tu > 1.3\% \end{cases}$$

$$(41) \quad F(\lambda_{\theta}) = \begin{cases} 1 + (12.986\lambda_{\theta} + 123.66\lambda_{\theta}^2 + 405.689\lambda_{\theta}^3) \exp[-(Tu/1.5)^{1.5}] & \text{if } \lambda_{\theta} \leq 0 \\ 1 + 0.275[1 - \exp(-35.0\lambda_{\theta})] \exp[-2Tu] & \text{if } \lambda_{\theta} > 0 \end{cases}$$

$$(47) \quad F_2 = \tanh \left[\max \left(2 \frac{\sqrt{\mathcal{K}}}{\beta^* \omega y}, \frac{500\nu}{y^2 \omega} \right)^2 \right]$$

$$(48) \quad \mu^F = \langle \rho \rangle_H C_v \Delta \sqrt{\mathcal{K}}.$$

The coefficients have been calibrated such that $a_1 = 0.31$ and $C_v = 0.0667$. These eddy viscosities are combined using the same blending equation as before:

$$(49) \quad \mu_T = \mathcal{F} \mu^E + (1 - \mathcal{F}) \mu^F.$$

Finally, a proper blending function \mathcal{F} that will switch from the RANS model to the LES model when appropriate must be selected. In the original hybrid RANS-LES model of Sánchez-Rocha^[15], the SST function F_2 defined in Eq. (47) is used. F_2 computes the ratio of the turbulence length scale $L_t \simeq \mathcal{K}^{3/2}/\varepsilon \simeq \mathcal{K}^{1/2}/(\beta^* \omega)$ to the distance to the nearest wall y . This ratio L_t/y is equal to approximately 2.5 in the logarithmic region of the boundary layer and reduces to zero towards the edge. The factor 2 in the first argument of Eq. (47) therefore ensures a smooth transition from a value of one in boundary-layers to zero for free shear layers. This blending function ($\mathcal{F} = F_2$) provided excellent results for massively separated flow on complex rotorcraft configurations^[1, 16, 38].

A shortcoming of this approach is that the freestream region is computed using LES without applying the required grid resolution or correct boundary conditions. When computing the flow past a flat plate using hybrid RANS-LES or LES for example, it is fundamental to provide realistic turbulent inflow conditions^[39]. Such approach is however not realistic for most external aerodynamic problems, where large cells are typically employed in the far field. It follows that the turbulent decay from the inlet to the geometry of interest is captured by a dramatically under-resolved LES. For regular Hybrid RANS-LES models, the impact on the results is usually negligible due to their low sensitivity with respect to turbulent boundary conditions. For a transitional model however, capturing the correct turbulent decay is key to accurately predict bypass transition cases, when the natural transition mechanism (Tollmien-Schlichting waves, etc) is bypassed such that the turbulent spots are directly

produced within the boundary layer by the freestream turbulence. It should be noted that this issue is not limited to hybrid RANS-LES methods based on the hybrid operator. DES models will also experience this unphysical decay, so that appropriate measures should be taken to ensure that the turbulent length scale recovers its RANS value away from the body. It is also important to realize that with LES models, it is not possible to modify the boundary conditions to match a given turbulence decay, as can be accomplished using RANS models^[29]. This is primarily because the destruction term in the RANS model depends on the solution only, while the LES destruction term also depends on the local grid spacing. It naturally follows that different grids will provide different rates of turbulent decay.

For the present model, it was decided to modify the blending function \mathcal{F} to make sure that the freestream decay would be captured using the RANS model and not the LES model. This is physically more realistic as RANS closures have been specifically calibrated for this types of flows. A freestream indicator to identify the regions where the blending function should switch back to RANS mode ($\mathcal{F} \rightarrow 1$) is therefore required. Such a sensor has already been developed within the original $\gamma - \overline{Re}_{\theta}$ model as the F_{θ} function defined in Eq. (43). The present switch is modified to remain active in wakes, so that

$$(50) \quad F_4 = 1 - \min \left[\max \left\{ e^{-\left(\frac{y}{c_4 \delta}\right)^4}, 1.0 - \left(\frac{\gamma - 1/c_{e2}}{1 - 1/c_{e2}}\right)^2 \right\}, 1.0 \right],$$

where c_4 controls the extent of the freestream region, as illustrated in Fig.1. In the present work, a value of $c_4 = 2$ was selected to ensure that the model would not switch back to RANS in sensitive wake regions, while capturing the inflow freestream using properly calibrated RANS models.

A final precaution is required to ensure that the blending function \mathcal{F} does not switch back to LES mode in laminar regions. In the original Lantry-Menter model^[4], the blending function F_1 defined in Eq. (22) is protected in laminar region by the F_3 function. A similar approach is adopted here, where the final blending function is defined as

$$(51) \quad \mathcal{F} = \max(F_2; F_3; F_4).$$

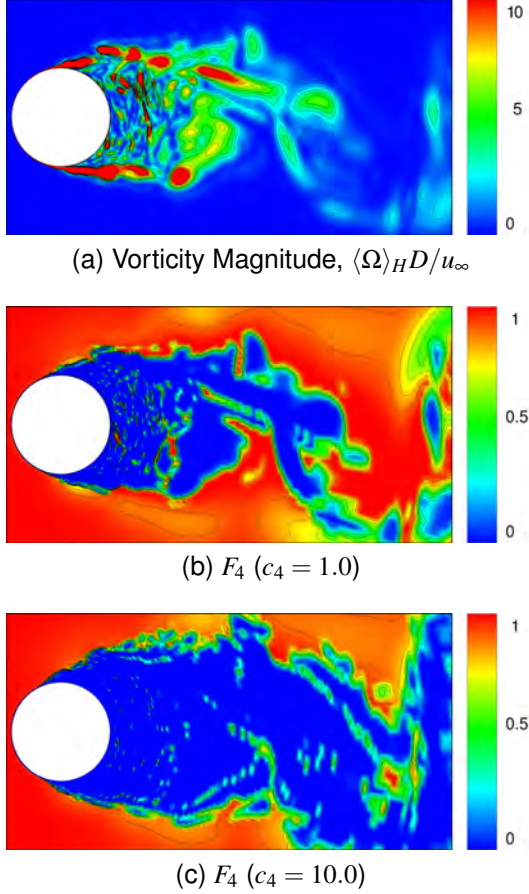


Fig. 1: Freestream sensor on a circular cylinder at $Re_D = 10^5$ and $M_\infty = 0.1$.

The boundary conditions for the new transitional hybrid RANS-LES model are similar to that of the original correlation-based approach. Freestream values at the inlet are enforced for \mathcal{K} and ω as suggested by Menter^[30] and can be adjusted to match the a specific turbulent decay. At the walls, the usual RANS boundary conditions are recovered, such that

$$(52) \quad \mathcal{K}_{wall} = 0 \quad ; \quad \omega_{wall} = 10 \frac{6\nu}{\beta_1 y_1^2},$$

where y_1 is the distance from the center of the first cell to the nearest wall. The hybrid turbulent kinetic energy and specific dissipation rate are simply extrapolated from the interior solution at the outlets. Regarding the two transitional variables γ and $\overline{Re_{\theta_i}}$, a zero-flux type condition is imposed at viscous walls. At the outlets, both variables are also extrapolated from the interior domain, while at inlets:

$$(53) \quad \gamma_\infty = 1 \quad \text{and} \quad \overline{Re_{\theta_i}} = R_{\theta_i}(\lambda_{\theta_i}, Tu_\infty).$$

Finally, it is important to understand that this transition model is not Galilean invariant, since the calculations of Tu and $d\langle U \rangle_H / ds$ rely on the velocity magnitude $\langle U \rangle_H$. In the case of moving body configurations, the

velocity relative to the nearest wall must be computed within the simulation.

3 RESULTS AND DISCUSSION

3.1 Numerical Method

A numerical solver has been developed at Georgia Tech to study complex rotorcraft problems such as dynamic stall and blades in reverse flow. This new platform was specifically designed to rapidly implement and evaluate state-of-the-art turbulence approaches. The three-dimensional compressible governing equations are solved in a time-accurate manner using a cell-centered finite volume approach on structured grid topologies. The spatial reconstruction is carried out using Van Leer's MUSCL scheme, leading to second-order accuracy. The convective fluxes are computed using Roe's flux difference splitting scheme, while the viscous fluxes are obtained from second-order central differences. The solution is marched in time using the implicit LU-SW scheme combined with the method of Gear to achieve second-order temporal accuracy. The number of Newton sub-iterations at each physical time step is chosen to ensure a proper convergence of the residuals^[40]. A large number of boundary conditions has been implemented, including inviscid/viscous walls, non-reflecting inlets/outlets based on Riemann invariants, etc. The solver is fully parallel (MPI) and includes rigid body rotation/translation using the Arbitrary Lagrangian Eulerian approach. The turbulent equations are solved in a loosely coupled manner in order to simplify the implementation of new models within the code. The proper implementation of the solver has been verified over a large number of test cases, ranging from laminar flat plates to dynamically pitching wings in reverse flow^[16].

3.2 Transitional Flow Past a Flat Plate

The new transitional hybrid RANS-LES closure is applied to the ERCOFTAC (European Research Community on Flow, Turbulence and Combustion) T3 series of transitional flat plate cases (see Table 1)^[41]. These experiments were conducted with turbulence

Table 1: Inlet conditions for the ERCOFTAC T3 cases^[41]. The turbulent eddy viscosity ratios are from Reference 29.

Case	Re_L	Tu [%]	μ_T / μ
T3A	6.12×10^5	3.3	12.0
T3B	1.07×10^6	6.5	100.0
T3A-	2.24×10^6	0.874	8.72
TSK	5.68×10^6	0.18	1.0

intensities of 1% or higher at the leading edge, so that bypass transition is the dominant transition mode. The experiment of Schubauer & Klebanoff^[42] was included in this study to verify the model's ability to predict natural transition (case TSK). The present transitional hybrid RANS-LES model was specifically developed to ensure that attached boundary layers would be resolved using the $\gamma - \overline{Re}_{\theta_i}$ model only, so that realistic turbulent conditions at the inlet should not be required. This assumption is investigated in this section, where the new model's capability to predict "steady" transitional flows is assessed.

The computational mesh consists of 399 points in the streamwise direction (350 of which lie on the flat plate) and 100 points in the normal direction. The inlet was located 0.15 grid units upstream of the leading edge, with a flat plate length of 1.7 units. In the normal direction, the farfield was located 0.3 units away from the wall, corresponding to approximately 8δ for the lowest Reynolds number, assuming a fully turbulent boundary layer. The wall spacing was chosen to ensure that $y^+ < 1$ over the entire flat plate even at the highest Reynolds number, with at least 30 points resolving the laminar boundary layer. A three-dimensional grid with $z^+ < 100$ and 50 points in the spanwise direction was generated, but as expected, the solver converged to a two-dimensional solution due to the absence of turbulent fluctuations.

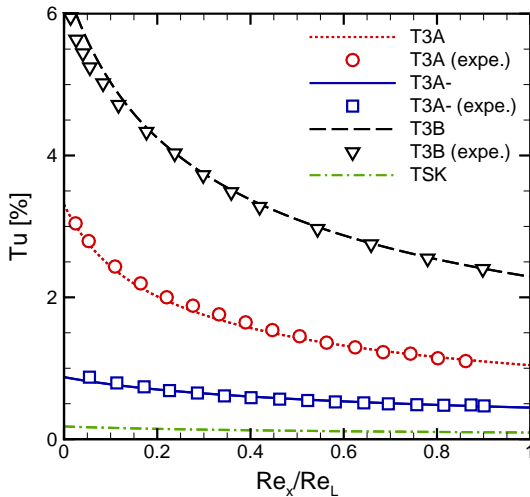


Fig. 2: Freestream turbulence decay for the zero pressure gradient flat plate simulations. Experimental data are from Reference 41.

The turbulence intensity and eddy viscosity ratio at the inlet must be carefully determined to match the experimental freestream turbulence decay. The turbulent viscosity ratios for the various cases are provided by Langtry^[29], and the inlet turbulence intensity is ob-

tained from a trial and error process. The freestream turbulence decay for all four cases is shown in Fig. 2. The skin friction distributions for the ERCOFTAC cases predicted by the present solver are illustrated in Fig. 3, along with the corresponding experimental data. The transition location, characterized by a

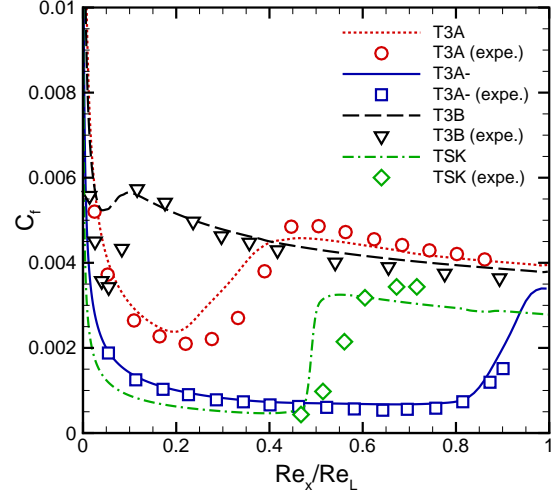


Fig. 3: Skin friction predictions for the ERCOFTAC cases. Experimental data are from Reference 41.

sharp rise in the wall shear stress, is correctly captured for all four cases. The results are typical of skin friction distributions predicted using the correlation-based transition model of Langtry and Menter^[4,31]. It is important to remember that high level of accuracy between the CFD and agreement with experiments obtained in the original paper is due to the fact that the correlations Eqs. (30) and (31) were calibrated using these T3 cases. These calibrations will not be perfectly correlated when applied to other CFD codes, so that discrepancies in the transition predictions are to be expected, as observed by Content^[43]. In order to further improve the agreement with experimental data in Fig. 3, the empirical correlations will be specifically developed for the present solver (in the future), using one of the methods available in the literature^[32,43,44].

Finally, the behaviour of the blending function \mathcal{F} within the transitional boundary layer is investigated. In laminar and freestream regions, the hybrid RANS-LES approach properly recovers the correlation-based model, with values of \mathcal{F} close to 1.0. A closer inspection was given to the outer region of the turbulent boundary layer where the blending function F_2 in Eq. (47) vanishes, being progressively replaced by F_4 from Eq. (50). Ideally, the blending function \mathcal{F} would remain equal to one throughout the entire boundary layer, leaving the flow resolution to the correlation-based model instead of the

LDKM. Indeed, hybrid RANS-LES models were initially developed to make the best of existing RANS models, while improving on their weaknesses using LES-based closures. For attached boundary layers, it would make little sense to resolve the entire flow field with LDKM, knowing that the $\gamma - \overline{Re_{\theta_i}}$ model is capable of predicting the transition just as accurately, for a fraction of the cost. The proper behavior of the present model is confirmed in Fig. 4, where the streamwise velocity profile in the turbulent boundary layer (case T3B at $Re_x = 10^6$) alongside the blending function \mathcal{F} . The local skin friction coefficient at this point is predicted within 2% of the experimental data while the velocity profile matches well the law-of-the-wall theory with $\kappa = 0.41$ and $B = 5.0$. The blending

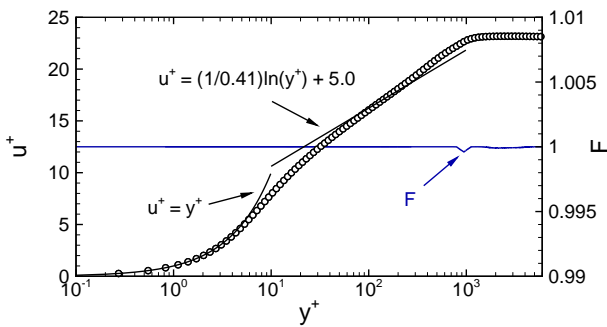


Fig. 4: Streamwise velocity profile at $Re_x = 10^6$ with the corresponding blending function \mathcal{F} for the T3B case.

function \mathcal{F} behaves as expected, with a negligible reduction (0.001%) at the edge of the boundary layer ($y^+ \simeq 1000$).

The new transitional hybrid RANS-LES model correctly captures natural and bypass transition in "steady" two-dimensional environments. The approach recovers the correlation-based model so that realistic turbulent inflow conditions and three-dimensional grids are not required.

3.3 Transitional Flow Past a Circular Cylinder

The transitional hybrid RANS-LES closure is now applied to a more complex configuration: the flow past a semi-infinite circular cylinder. Despite its geometrical simplicity, this test case remains a serious challenge for numerical simulations as it contains both massively separated flows and transitional boundary layers. This complex aerodynamic environment is perfectly suited to evaluate the new hybrid transitional approach. The Reynolds number based on the cylinder diameter D was increased from 10 to 2×10^6 to capture a wide range of flow regimes, from creeping to almost post-critical. The simulations were run

with a freestream Mach number $M_\infty = 0.1$ so that the flow field remains incompressible, but the compressible solver is not overly constrained. The maximum local change in density was found to remain constantly below 1.1%, hence confirming that compressibility effects were negligible in the present study. Four different turbulence models were used to simulate this configuration: The original $k - \omega$ SST^[30] and $\gamma - \overline{Re_{\theta_i}}$ ^[4] models, as well as the baseline hybrid RANS-LES model of Sanchez-Rocha^[15] and the transitional hybrid closure proposed in this paper.

The computational domain extends approximately $50 \times D$ all around the cylinder and the spanwise width is $2 \times D$ with periodic boundary conditions. Each cylindrical section was meshed using a structured O-grid, spanned by $(256 \times 128 \times 295)$ points in the azimuthal, spanwise and radial directions, respectively. The grid spacing at the wall corresponds to $y^+ < 1$ for the highest Reynolds number, with at least 50 points resolving the boundary layer^[45]. The simulations were accomplished with a physical time-step $\Delta t \times u_\infty \times D = 0.01$, yielding approximately 200 iterations per vortex shedding cycle. The number of sub-iterations was then defined to ensure a residual drop of at least two orders of magnitude between each time step. For the transition model, the boundary values were adjusted to provide a turbulence intensity around 0.05% at the cylinder to ensure that bypass transition would not perturb the simulation.

Comparing the mean drag coefficient as a function of Reynolds number in Fig. 5, the proposed transitional hybrid RANS-LES approach is observed to capture the drag crisis more accurately than the other models. Not surprisingly, all four models pro-

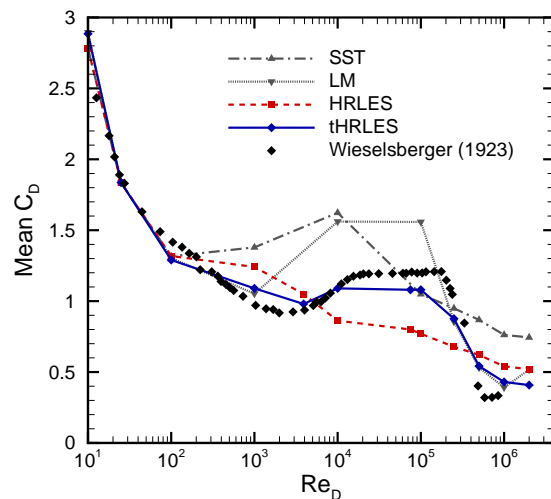


Fig. 5: Mean drag predictions using four turbulence closures on a circular cylinder in crossflow.

vide results in close agreement with the experimental data at low Reynolds numbers ($Re_D < 100$). As the Reynolds number is further increased, both URANS models begin to fail, reaching mean drag coefficients of approximately 1.6 at $Re_D = 10^4$. This inability to predict massively separated boundary layers is a known issue of RANS models [46], as the low-pressure region is dramatically over-predicted at the back of the cylinder, resulting in excessive drag predictions. The force predicted by the SST model decreases below the $\gamma - \overline{Re_\theta}$ level, as its fully turbulent boundary layer remains attached over a longer portion of the cylinder. A similar behavior is observed for the hybrid RANS-LES model, which completely smoothes out the transition process. The mean drag predictions are largely under-predicted as the turbulent boundary layer is more resistant to adverse pressure gradients. Nevertheless, the unphysical suction predicted by the RANS approaches is not obtained with the hybrid model, yielding more realistic values for the forces acting on the cylinder. The transition process is properly captured by the correlation-based model, but as previously mentioned, the suction on the aft portion of the cylinder is dramatically over-predicted around $Re_D = 10^4$. Finally, the proposed hybrid RANS-LES closure appears to combine the best of both worlds: the transition process is properly captured at $Re_D \simeq 2 \times 10^5$ but the unphysical suction is avoided by the LES hybridization. The new approach provides results in close agreement with the experimental data over the entire range of Reynolds numbers, from the creeping regime all the way to the supercritical regime.

At the lowest Reynolds numbers, a steady two-dimensional solution is obtained with a small separated region on the aft part of the cylinder. As the Reynolds number is increased to 100, the separation bubble becomes unstable and a Von Karman vortex street begins to form without any spanwise variation. Up to this point, the flow field is entirely laminar and is therefore being captured using the correlation-based model only ($\mathcal{F} \rightarrow 1$). Beyond this value, the laminar boundary layer separates around 80° and transition to turbulence occurs in the wake of the cylinder, which becomes highly three-dimensional. This phenomenon is clearly illustrated in Fig. 6, where contours of intermittency are displayed on iso-surfaces of vorticity magnitude at various Reynolds numbers. The spanwise fluctuations become fully apparent at $Re_D = 10^4$, as the wake transitions to turbulence approximately one diameter downstream of the cylinder. As expected from the turbulent energy cascade, the higher Reynolds number cases exhibit higher frequency content in the immediate wake of the cylinder. At the highest Reynolds number simulated ($Re_D = 2 \times 10^6$), the boundary layer has already transitioned prior to separating, resulting in a fully turbulent wake.

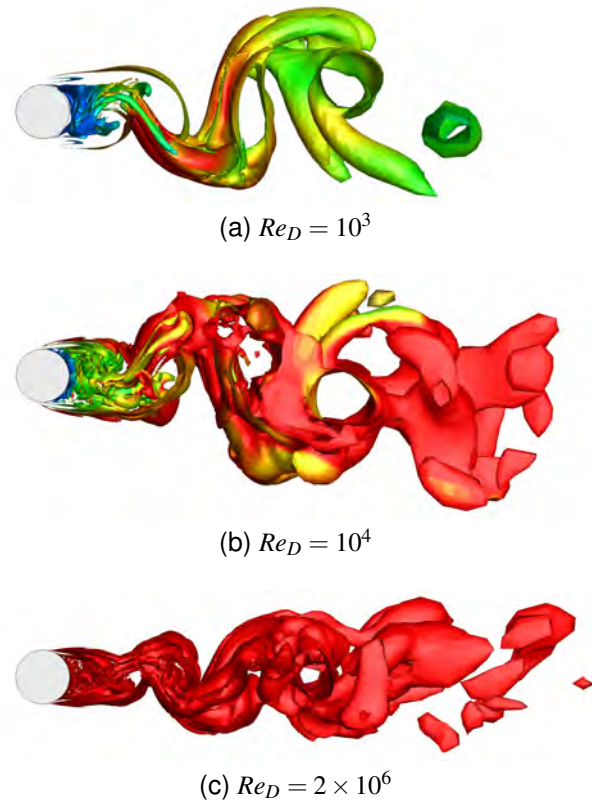


Fig. 6: Instantaneous contours of intermittency displayed on iso-surfaces of vorticity magnitude (Transitional hybrid RANS-LES predictions on circular cylinders at various Reynolds numbers)

The wake also appears to lose its coherence as the Reynolds number increases, so that the large structures observed at $Re_D = 10^3$ are barely visible at $Re_D = 2 \times 10^6$.

Figure 7 illustrates the limiting streamlines near the cylinder surface superimposed with contours of intermittency in the boundary layer. This graph provides useful insight regarding the exact transition physics captured by the model at various Reynolds numbers during the drag crisis. For a Reynolds number of 10^4 , the entire cylinder surface remains laminar as the transition to turbulence occurs further downstream in the wake, as shown in Fig. 6. At a Reynolds number of 2.5×10^5 , the laminar boundary layer still separates, but transition occurs immediately after the separation line. Beyond that value, the transition process occurs directly on the surface of the cylinder, followed by turbulent separation of the boundary layer further downstream. As the Reynolds number is increased, the extent of the attached flow region also increases due to the greater resistance of turbulent boundary layer with respect to adverse pressure gradients. This phenomenon is illustrated in Fig. 7, where the instantaneous contours of vorticity magnitude have been plotted, showing a clear narrowing of the wake for higher Reynolds numbers.

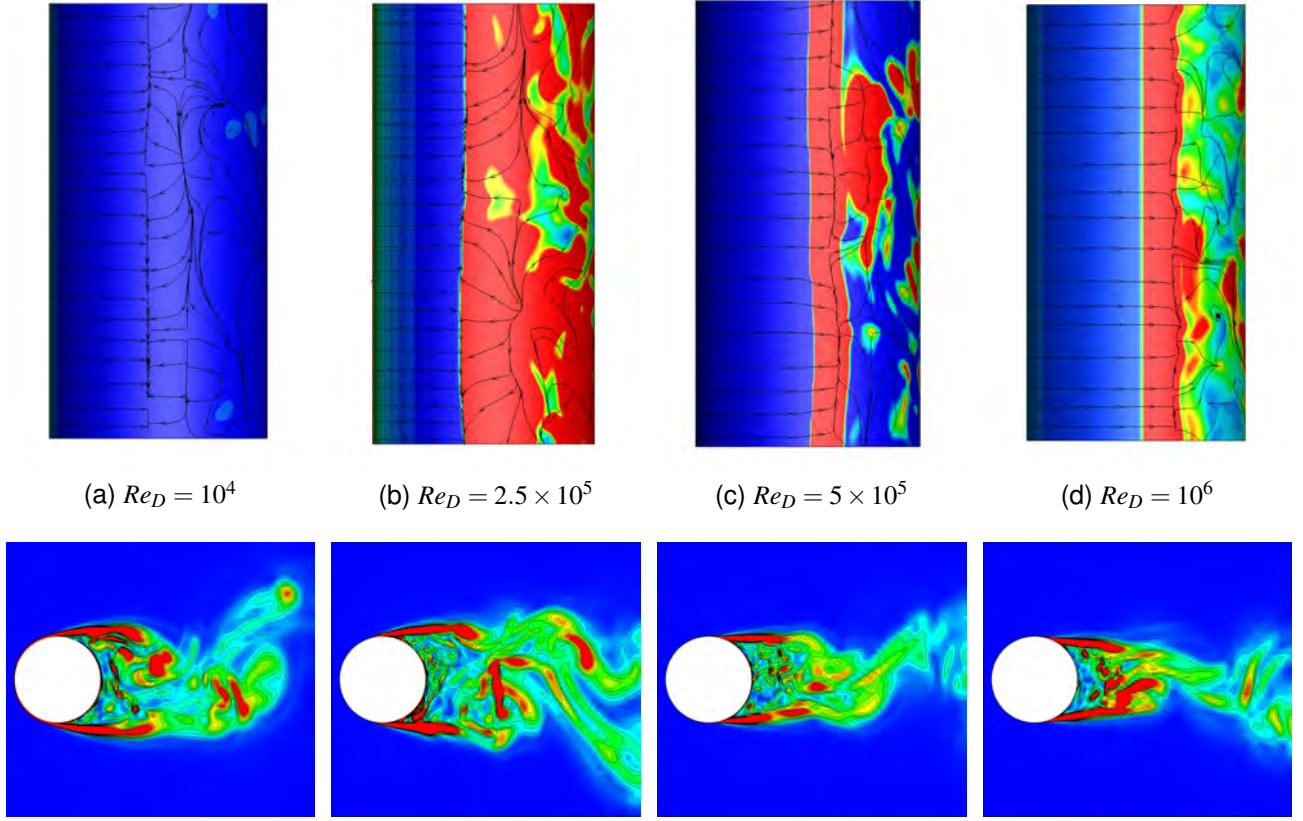


Fig. 7: Top view of instantaneous streamlines on a semi-infinite circular cylinder, superimposed with contours of intermimency γ near the surface (top row). Instantaneous contours of vorticity magnitude (bottom row).

The statistics of the circular cylinder at $Re_D = 3,900$ have been further investigated, due to the availability of both LES^[20] and experimental data^[47] (measured at $Re_D = 5,000$) in the literature. The results have been summarized in Table 2. The $k - \omega$ SST

Table 2: Statistics predicted by various turbulence models for a circular cylinder at $Re_D = 3,900$. LES and experimental data are from References 20 and 47

Model	Mean C_D	Strouhal no.	Sep. Angle
SST	1.58	0.238	98.4°
HRLES	1.05	0.210	86.7°
LES	1.04	0.210	88.0°
LM	1.35	0.230	96.5°
tHRLES	1.03	0.209	88.0°
Expe.	0.99 ± 0.05	0.215 ± 0.005	$86^\circ \pm 2^\circ$

and Langtry-Menter models strongly over-predict the base suction, leading to a drag coefficient 50% higher than the experimental value. The LES-based models capture the pressure distribution and separation location, so that the drag coefficient falls within the experimental range (see Table 2). The URANS mod-

els do not capture the flow features that were measured experimentally, and the shedding frequency is over-predicted by as much as 13%. The HRLES and tHRLES closures provide a much better prediction for the shedding frequency, in excellent agreement with both the LES data of Beaudan^[20] and the experimental measurements of Son^[47].

In addition to verifying integrated quantities such as the drag coefficient, the mean streamwise velocity profiles u/U_∞ were also compared to experimental data^[48] at seven downstream locations. The results have been plotted in Fig. 8, where x and z denote the streamwise and transverse directions, respectively. The dissipative nature of RANS models becomes evident as the flow travels further downstream. Only half a diameter downstream of the cylinder ($x/D = 1.06$), the peak velocity predicted by the $k - \omega$ SST model is already 60% lower than the experimental value. Conversely, the tHRLES and HRLES models provide a very accurate velocity profile even in the far wake ($x/D = 10$), where the peak value is still captured within 9%. The HRLES provides very accurate predictions for this configuration, despite being a fully turbulent model. This is because the flow at this moderate Reynolds number is dominated by the large

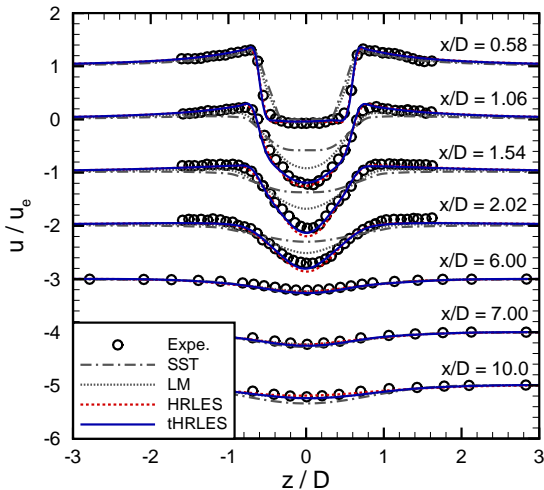


Fig. 8: Streamwise velocity profiles at several downstream locations behind a circular cylinder at $Re_D = 3,900$. Experimental data is from Reference 48. Starting with $x/D = 1.06$, each successive profile has been translated in u/U_∞ by -1 .

adverse pressure gradient on the cylinder, leading to massive boundary layer separation (close to 90°). As the Reynolds number is increased, the HRLES predictions become less accurate while the transitional HRLES model retains its accuracy, as shown in Fig. 5.

3.4 Transitional Flow Past a NACA 63-415 Wing

Finally, the flow past a semi-infinite NACA 63-415 wing is evaluated using the new transitional hybrid RANS-LES model. This airfoil is frequently used on wind turbine blades, with an operational Reynolds number based on the chord $Re_c = 3 \times 10^6$. This configuration is also relevant to helicopter aerodynamics, as such conditions are likely to be encountered near the rotor root. The numerical simulations were conducted using both the new transitional model and the standard HRLES model, as well as XFOIL predictions based on the e^N method. The turbulence freestream intensity was set to approximately 0.05%, which corresponds to natural transition. The flow field is essentially incompressible ($M_\infty = 0.1$), while the incidence varies from -10° to 15° . The C-type mesh extends approximately $50 \times c$ around the wing, with 897 points in the circumferential direction (600 of which lie on the airfoil), 64 points in the spanwise direction ($z^+ \sim 200$) and 160 points in the normal direction. The grid spacing at the wall corresponds to $y^+ < 1$ with approximately 50 points resolving the boundary layer. The physical time step is $\Delta t \times u_\infty \times c = 0.01$, with enough subiterations to reduce the L_∞ norm of the residuals

by at least two orders of magnitude between each iteration.

The lift and drag coefficients predicted by the various models are compared to experimental data in Fig. 9. The lift coefficient is accurately captured by all turbulent closures, with negligible transitional effects on the pressure distributions of the airfoil. For the drag coefficient, transitional effects become significant, in particular at low angles of attack where viscous drag dominates. The new transitional approach provides results in much better agreement with experimental results compared to the traditional HRLES closure. The predictions based on the e^N method are similarly accurate, but this approach is limited to relatively simple geometries [29], while the proposed model can be applied to a wide range of complex configurations.

Neither the baseline nor transitional models capture the stall location exactly in Fig. 9. This failure of the turbulence closures was expected as stall predictions have been shown to be very sensitive to parameters such as turbulence freestream intensity and surface roughness [33]. The new transitional model in this limited application appears to improve the early separation found in the original HRLES model, but further studies are necessary. The capability of the model for predicting massively separated boundary layers has already been established in the previous section with a transitional cylinder in crossflow. This NACA 63-415 configuration at moderate angles of attack was instead designed to verify that the three-dimensional hybrid model would recover its two-dimensional RANS solution for attached boundary layers undergoing severe pressure gradients. This was confirmed by running both two- and three-dimensional simulations which converged to identical solutions, in agreement with their respective RANS models. Capturing the onset flow separation using hybrid RANS-LES closure requires an accurate model for the transfer of momentum and energy throughout the boundary layer, which is still incomplete due to the absence of the hybrid terms in the present model. Future studies will include these terms as described in the previous sections and investigate their impact on the results at higher angles of attack in the stalled regime.

3.5 Computational Cost

Finally, the computational cost of the proposed transitional hybrid RANS-LES model is compared to that of other well-known turbulence closures. Each approach was applied to the same three-dimensional configuration and the simulations were run on the same machine with identical inputs to ensure a fair comparison. The results relative to the baseline (no turbulence model) are shown in Table 3. As expected, the

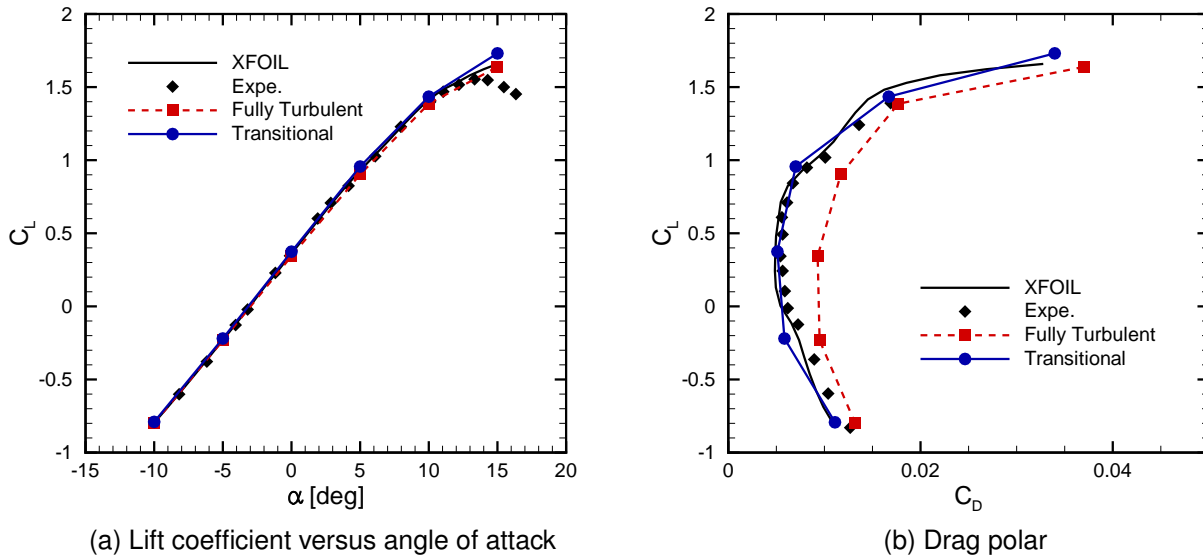


Fig. 9: Numerical predictions for a semi-infinite NACA 63-415 wing at $Re_c = 3 \times 10^6$. Experimental data are from Reference 49.

Table 3: Execution time and memory requirements for various turbulence closures.

Turbulence	Exec. Time	Mem. Req.
No model	1.00	1.00
SST	1.28	1.28
HRLES	1.29	1.31
LM	1.69	1.58
tHRLES	1.71	1.69

computational cost and memory requirements are primarily driven by the number of additional partial differential equations in the turbulence model. In the present code, these equations are solved in a loosely coupled manner using an implicit LU-SW scheme. Although the state vector size is increased due to the additional conserved variables such as the turbulent kinetic energy k or specific dissipation rate ω , the main increase in memory requirements comes from the larger flux Jacobian matrix. The convective part of the implicit block is computed using first-order Steger & Warming fluxes so that the entire Jacobian matrix is stored at each face. This represents seven $N \times N$ matrices per cell, where N is the number of additional partial differential equations in the model. It is therefore worth mentioning that the results presented in Table 3 are dependent on the model implementation. If the convective flux Jacobian is approximated with the spectral radius for example, there is no more need to store the implicit block, so that the memory requirements will drop considerably. This approximation was

not implemented here because of its low convergence rate on high aspect ratio grids.

The computational costs of the hybrid RANS-LES models are only slightly higher than the costs of the RANS models they are based on. This is mostly due to the fact that the blending only occurs in the turbulent kinetic energy equation, requiring only a few extra terms to be computed while all the gradients are already available. The major computational cost increase does not actually appear explicitly in Table 3, that is, LES-based models must be run on three-dimensional grids with fine time steps to resolve about 80% of the turbulent spectrum in the LES regions. Furthermore, the total simulation time is usually increased significantly to allow a proper reconstruction of the flow statistics from the instantaneous turbulent data.

4 CONCLUSION

A new turbulence approach has been proposed, that combines the strengths of the local dynamic kinetic model (LDKM) and the widely adopted $\gamma - \overline{Re_\theta}$ transition model. Preliminary studies on a transitional flat plate and semi-infinite NACA 63-415 wing have established that the proposed model properly recovered its baseline URANS model for attached boundary layers. Further simulations on a circular cylinder in crossflow at various Reynolds numbers confirm that the new approach significantly improves the stall predictions as it switches to large eddy simulations in

wakes and separated regions. The model was found to be numerically robust and requires less than 2% extra computational work per iteration as compared to the baseline transition model. Now that the proper numerical behavior of the transitional hybrid RANS-LES closure has been established, future studies will concentrate on improving its predictive capabilities. In particular, the hybrid terms that were neglected in the present paper will be re-introduced and their impact on the solution investigated, with an emphasis on the stall onset regime, where the sensitivity to the transfer of momentum and energy throughout the boundary layer is maximum. Three-dimensional crossflow terms will also be investigated for both rotor and fuselage conditions.

ACKNOWLEDGEMENTS

The investigation was supported by the U.S. Army/Navy/NASA Vertical Lift Research Center of Excellence with Mahendra Bhagwat serving as Program Manager and Technical Agent, grant number W911W6-11-2-0010. The authors would also like to thank Professor Suresh Menon from the Georgia Institute of Technology, for computational access to his high performance computers.

The U.S. Government is authorized to reproduce and distribute reprints notwithstanding any copyright notation thereon. The views and conclusions contained in this document are those of the authors and should not be interpreted as representing the official policies, either expressed or implied, of the U.S. Government.

COPYRIGHT STATEMENT

The authors confirm that they, and/or their company or organization, hold copyright on all of the original material included in this paper. The authors also confirm that they have obtained permission, from the copyright holder of any third party material included in this paper, to publish it as part of their paper. The authors confirm that they give permission, or have obtained permission from the copyright holder of this paper, for the publication and distribution of this paper as part of the ERF 2015 proceedings or as individual off-prints from the proceedings.

REFERENCES

[1] Shenoy, R., Holmes, M., Smith, M., and Komerath, N., "Scaling Evaluations on the Drag of a Hub System," *Journal of the American Helicopter Society*, Vol. 58, (3), 2013, pp. 1–13.

[2] Pape, A. L., Richez, F., and Deck, S., "Zonal Detached-Eddy Simulation of an Airfoil in Post-stall Condition," *AIAA Journal*, Vol. 51, (8), 2013, pp. 1919–1931.

[3] Spalart, P. R., "Detached-Eddy Simulation," *Annual Review of Fluid Mechanics*, Vol. 41, 2009, pp. 181–202.

[4] Langtry, R. and Menter, F., "Correlation-Based Transition Modeling for Unstructured Parallelized Computational Fluid Dynamics Codes," *AIAA Journal*, Vol. 47, (12), 2009, pp. 2894–2906.

[5] Medida, S. and Baeder, J. D., "Application of the Correlation-based γ - Re_{θ_t} Transition Model to the Spalart-Allmaras Turbulence Model (AIAA Paper 2011-3979)," 20th AIAA Computational Fluid Dynamics Conference, June 2011.

[6] Seyfert, C. and Krumbein, A., "Evaluation of a Correlation-based Transition Model and Comparison with the e^N method," *Journal of Aircraft*, Vol. 49, (6), 2012, pp. 1765–1773.

[7] Spalart, P. R., "Strategies for Turbulence Modelling and Simulations," *International Journal of Heat and Fluid Flow*, Vol. 21, (3), 2000, pp. 252–263.

[8] Fröhlich, J. and von Terzi, D., "Hybrid LES/RANS Methods for the Simulation of Turbulent Flows," *Progress in Aerospace Sciences*, Vol. 44, (5), 2008, pp. 349–377.

[9] Spalart, P. R., Deck, S., Shur, M., Squires, K., Strelets, M. K., and Travin, A., "A New Version of Detached-Eddy Simulation, Resistant to Ambiguous Grid Densities," *Theoretical and Computational Fluid Dynamics*, Vol. 20, (3), 2006, pp. 181–195.

[10] Shur, M. L., Spalart, P. R., Strelets, M. K., and Travin, A. K., "A Hybrid RANS-LES Approach with Delayed-DES and Wall-Modelled LES Capabilities," *International Journal of Heat and Fluid Flow*, Vol. 29, (6), 2008, pp. 1638–1649.

[11] Piomelli, U., Balaras, E., Pasinato, H., Squires, K. D., and Spalart, P. R., "The Inner–Outer Layer Interface in Large-Eddy Simulations with Wall-Layer Models," *International Journal of Heat and Fluid Flow*, Vol. 24, (4), 2003, pp. 538–550.

[12] Deck, S., "Recent Improvements in the Zonal Detached Eddy Simulation (ZDES) Formulation," *Theoretical and Computational Fluid Dynamics*, Vol. 26, (6), 2012, pp. 523–550.

[13] Germano, M., "Properties of the Hybrid RANS/LES Filter," *Theoretical and Computational Fluid Dynamics*, Vol. 17, (4), 2004, pp. 225–231.

[14] Germano, M., "On the Hybrid RANS-LES of Compressible Flows," *Progress in Hybrid RANS-LES Modelling*, Springer, 2015, pp. 253–263.

- [15] Sánchez-Rocha, M. and Menon, S., "The Compressible Hybrid RANS/LES Formulation Using an Additive Operator," *Journal of Computational Physics*, Vol. 228, (6), 2009, pp. 2037–2062.
- [16] Hodara, J., Lind, A., Jones, A., and Smith, M., "Collaborative Investigation of the Aerodynamic Behavior of Airfoils in Reverse Flow (AHS Paper 2015-267)," 71st AHS Forum, May 2015.
- [17] Comte, F. D., Lesieur, M., *et al.*, "Large-Eddy Simulation of Transition to Turbulence in a Boundary Layer Developing Spatially Over a Flat Plate," *Journal of Fluid Mechanics*, Vol. 326, 1996, pp. 1–36.
- [18] Monokrousos, A., Brandt, L., Schlatter, P., and Henningson, D., "Ten Years of Industrial Experience with the SST Turbulence Model," *International Journal of Heat and Fluid Flow*, Vol. 29, 2008, pp. 841–855.
- [19] Germano, M., Piomelli, U., Moin, P., and Cabot, W. H., "A Dynamic Subgrid-Scale Eddy Viscosity Model," *Physics of Fluids A: Fluid Dynamics*, Vol. 3, (7), 1991, pp. 1760–1765.
- [20] Beaudan, P. and Moin, P., "Numerical Experiments on the Flow Past a Circular Cylinder at Sub-Critical Reynolds Number," Technical report, Office of Naval Research, Report No. TF-62, 1994.
- [21] Michelassi, V., Wissink, J., Fr-ogrove, J., hlich, and Rodi, W., "Large-Eddy Simulation of Flow Around Low-Pressure Turbine Blade with Incoming Wakes," *AIAA journal*, Vol. 41, (11), 2003, pp. 2143–2156.
- [22] Smith, A. M. O. and Gamberoni, N., "Transition, Pressure Gradient and Stability Theory," Technical report, Douglas Aircraft Company, El Segundo Division, 1956.
- [23] Krumbein, A., Krimmelbein, N., and Schrauf, G., "Automatic Transition Prediction in Hybrid Flow Solver, Part 1: Methodology and Sensitivities," *Journal of Aircraft*, Vol. 46, (4), 2009, pp. 1176–1190.
- [24] Eulitz, F. and Engel, K., "Numerical Investigation of Wake Interaction in a Low Pressure Turbine (Paper No. 98-GT-563)," ASME 1998 International Gas Turbine and Aeroengine Congress and Exhibition, 1998.
- [25] Nürnberger, D. and Greza, H., "Numerical Investigation of Unsteady Transitional Flows in Turbomachinery Components Based on a RANS Approach," *Flow, Turbulence and Combustion*, Vol. 69, (3-4), 2002, pp. 331–353.
- [26] Biswas, D. and Fukuyama, Y., "Calculation of Transitional Boundary Layers With an Improved Low-Reynolds-Number Version of the $k-\epsilon$ Turbulence Model," *Journal of Turbomachinery*, Vol. 116, (4), 1994, pp. 765–773.
- [27] Jones, W. and Launder, B., "The Calculation of Low-Reynolds-Number Phenomena With a Two-Equation Model of Turbulence," *International Journal of Heat and Mass Transfer*, Vol. 16, (6), 1973, pp. 1119–1130.
- [28] Mayle, R. and Schulz, A., "The Path to Predicting Bypass Transition," *Journal of Turbomachinery*, Vol. 119, (3), 1997, pp. 405–411.
- [29] Langtry, R. B., *A Correlation-Based Transition Model Using Local Variables for Unstructured Parallelized CFD Codes*, Ph.D. thesis, University of Stuttgart, 2006.
- [30] Menter, F. R., Kuntz, M., and Langtry, R., "Ten Years of Industrial Experience with the SST Turbulence Model," *Turbulence, Heat and Mass Transfer*, Vol. 4, 2003, pp. 625–632.
- [31] Benyahia, A., *Mise en Oeuvre et Evaluation d'un Modèle de Transition à Equations de Transport pour la Simulation d'Écoulements en Turbomachines*, Ph.D. thesis, Toulouse, ISAE, 2012.
- [32] Malan, P., Suluksna, K., and Juntasaro, E., "Calibrating the γ - Re_θ Transition Model for Commercial CFD," AIAA Paper 2009-1142 (Orlando, FL), 47th AIAA Aerospace Sciences Meeting, June 2009.
- [33] Sørensen, N. N., Bechmann, A., and Zahle, F., "3D CFD Computations of Transitional Flows Using DES and a Correlation Based Transition Model," *Wind Energy*, Vol. 14, (1), 2011, pp. 77–90.
- [34] Menon, S. and Patel, N., "Subgrid Modeling for Simulation of Spray Combustion in Large-Scale Combustors," *AIAA Journal*, Vol. 44, (4), 2006, pp. 709–723.
- [35] Aubry, N., "On the Hidden Beauty of the Proper Orthogonal Decomposition," *Theoretical and Computational Fluid Dynamics*, Vol. 2, (5-6), 1991, pp. 339–352.
- [36] Rajamani, B. and Kim, J., "A Hybrid-Filter Approach to Turbulence Simulation," *Flow, Turbulence and Combustion*, Vol. 85, (3-4), 2010, pp. 421–441.
- [37] Sánchez-Rocha, M. and Menon, S., "An Order-of-Magnitude Approximation for the Hybrid Terms in the Compressible Hybrid RANS/LES Governing Equations," *Journal of Turbulence*, Vol. 12, (16), 2011, pp. 1–22.
- [38] Sánchez-Rocha, M., Kirtas, M., and Menon, S., "Zonal Hybrid RANS-LES Method for Static and Oscillating Airfoils and Wings (AIAA Paper 2006-1256)," 44th AIAA Aerospace Sciences Meeting and Exhibit, Jan. 2006.

[39] Lund, T. S., Wu, X., and Squires, K. D., "Generation of Turbulent Inflow Data for Spatially-Developing Boundary Layer Simulations," *Journal of Computational Physics*, Vol. 140, (2), 1998, pp. 233–258.

[40] Smith, M. J., Jain, R., Grubb, A., and Jacobson, K., "Time- and Spatially-Adapting Simulations for Efficient Dynamic Stall Predictions," 41st European Rotorcraft Forum, September 1–4, 2015.

[41] Pironneau, O., Rodi, W., Ryming, I., Savill, A., and Truong, T., *Numerical Simulation of Unsteady Flows and Transition to Turbulence*, Cambridge University Press, May 2008, Chapter A Synthesis of T3 Test Case Predictions.

[42] Schubauer, G. B. and Klebanoff, P., "Contributions on the Mechanics of Boundary-Layer Transition," Technical report, NACA TR-1289, National Advisory Committee for Aeronautics, January 1956.

[43] Content, C., *Methode Innovante pour le Calcul de la Transition Laminaire-Turbulent dans les Codes Navier-Stokes*, Ph.D. thesis, Toulouse, ISAE, 2011.

[44] Sørensen, N. N., "CFD Modelling of Laminar-Turbulent Transition for Airfoils and Rotors using the γ -model," *Wind Energy*, Vol. 12, (8), 2009, pp. 715–733.

[45] Liggett, N. and Smith, M. J., "Temporal Convergence Criteria for Time-Accurate Viscous Simulations of Separated Flows," *Computers & Fluids*, Vol. 66, 2012, pp. 140–156.
doi: 10.1016/j.compfluid.2012.06.010

[46] Smith, M. J., Liggett, N., and Koukol, B. C. G., "The Aerodynamics of Airfoils at High and Reverse Angles of Attack," *AIAA Journal of Aircraft*, Vol. 48, (6), 2011, pp. 2012–2023.
doi: 10.2514/1.55358

[47] Son, J. S. and Hanratty, T. J., "Velocity Gradients at the Wall for Flow Around a Cylinder at Reynolds Numbers from 5×10^3 to 10^5 ," *Journal of Fluid Mechanics*, Vol. 35, (2), 1969, pp. 353–368.

[48] Ong, L. and Wallace, J., "The Velocity Field of the Turbulent Very Near Wake of a Circular Cylinder," *Experiments in Fluids*, Vol. 20, (6), 1996, pp. 441–453.

[49] Abbott, I. H. and Von Doenhoff, A. E., *Theory of Wing Sections, Including a Summary of Airfoil Data*, Dover, 1959.